SCIENCE CHINA
Physics, Mechanics & Astronomy

• Article •

September 2023 Vol. 66 No. 9: 293011
https://doi.org/10.1007/s11433-023-2148-8

Efficient production of ultracold polar molecules $^{23}Na^{40}K$ in their absolute ground state via intermediate state of the coupled complex $B^1\Pi\ |v = 4\rangle \sim c^3\Sigma^+\ |v = 25\rangle$

Zi-Liang Li[1,2], Zheng-Yu Gu[1,2], Peng-Jun Wang[1,2*], and Jing Zhang[1,2*]

[1] *State Key Laboratory of Quantum Optics and Quantum Optics Devices, Institute of Opto-electronics, Shanxi University, Taiyuan 030006, China;*
[2] *Collaborative Innovation Center of Extreme Optics, Shanxi University, Taiyuan 030006, China*

Received February 19, 2023; accepted May 24, 2023; published online August 11, 2023

We report on the efficient creation of a sample of 2.2×10^4 fermionic polar molecules $^{23}Na^{40}K$ in their rovibrational ground state $X^1\Sigma^+\ |v = 0, J = 0\rangle$ at 247 nK via an intermediate state of the spin-orbit coupled complex $B^1\Pi\ |v = 4\rangle \sim c^3\Sigma^+\ |v = 25\rangle$. Compared with the intermediate state of the coupled complex $B^1\Pi\ |v = 12\rangle \sim c^3\Sigma^+\ |v = 35\rangle$, this intermediate state has the larger Franck-Condon factors for up- and down-leg coupling of stimulated Raman adiabatic passage (STIRAP). We demonstrate this two-photon pathway to the $^{23}Na^{40}K$ ground state molecules and find that the one-way STIRAP transfer efficiency reaches 75%. The molecules $^{23}Na^{40}K$ in their rovibrational ground state are an ideal candidate for the quantum simulation and quantum information of ultracold molecules with long-range interaction.

ultracold atoms, ultracold molecule, STIRAP

PACS number(s): 34.20.Cf, 67.85.Hj, 03.75.Lm

Citation: Z.-L. Li, Z.-Y. Gu, P.-J. Wang, and J. Zhang, Efficient production of ultracold polar molecules $^{23}Na^{40}K$ in their absolute ground state via intermediate state of the coupled complex $B^1\Pi\ |v = 4\rangle \sim c^3\Sigma^+\ |v = 25\rangle$, Sci. China-Phys. Mech. Astron. **66**, 293011 (2023), https://doi.org/10.1007/s11433-023-2148-8

1 Introduction

Ultracold polar molecules have complex internal structures and strong long-range interaction, providing an ideal physical platform for a wide range of applications in quantum science [1-10], such as many-body physics, strongly correlated quantum systems, ultracold chemistry, quantum computation, and precision measurement. Compared with the ultracold atoms, molecules possess vibrational and rotational degrees of freedom and behave differently from atoms, which allows them to repel or attract other molecules depending on their relative orientation similar to magnets. This feature expands the tool set available in research and supports the study to achieve full quantum state control, especially using a static or rotating electrical field to control [11]. However, this additional complexity in the molecule energy level means that cooling molecules to ultralow temperatures remains a big challenge despite there being rapid progress in cooling methods [12-14].

To date, associating the atoms in nK to molecules near a Feshbach resonance is the only way to obtain the molecular sample in the quantum degenerate regime where quantum effects become predominant [15]. The cooling technology for neutral atoms is very successful and has been used to cool many neutral atoms to the quantum degenerate regime, which gives us a route to creating the diatomic molecules

*Corresponding authors (Peng-Jun Wang, email: pengjun_wang@sxu.edu.cn; Jing Zhang, email: jzhang74@yahoo.com; jzhang74@sxu.edu.cn)

in nK regime. By this way, many bi-alkali molecules in the rovibrational ground state have been produced by the association of weakly bound Feshbach molecules from ultracold atoms and followed by STIRAP [16-25]. For studying the statistics property in the molecules application, the preparation of fermionic molecules is a key point. Recently, the fermionic polar molecules ^{87}Rb^{40}K and ^{23}Na^{40}K in the rovibrational ground state have been prepared in quantum degeneracy [22, 23, 26]. Many experimental techniques have been developed to increase the molecule creating efficiency, including producing a sample of a lot of atoms at lower temperature by gray molasses [22], higher creating efficiency of Feshbach molecules by magnetic association [20, 27, 28], loading into a species-dependent optical dipole trap [29], and selecting a Feshbach molecular state with a stretched singlet hyperfine component [25] and so on.

Based on whether the chemical reaction AB+AB→A_2+B_2 is endothermic or exothermic, there are only two chemically stable fermionic bi-alkali molecules ^{23}Na^{40}K with an electrical dipole moment d=2.73D and ^{133}Cs^{40}K with 2.58D [30-32]. However, the loss of ^{23}Na^{40}K molecules in the rovibrational ground state still was observed in experiments [19, 23], which is a challenge to fully understand the loss mechanism [33]. For creating the ^{23}Na^{40}K in their rovibrational ground state, transferring the Feshbach molecules to the ground state in the experiment employs an excited intermediate state in the mixed complex $B^1\Pi\ |v = 12\rangle \sim c^3\Sigma^+\ |v = 35\rangle$ with strong spin-orbit coupling strength ξ_{Bc}=0.58 cm^{-1} [19-21], or unresolved hyperfine structure in the $d^3\Pi$ potential [24].

In this paper, we report the creation of a sample of 2.2×10^4 fermionic molecules ^{23}Na^{40}K in their rovibrational ground state $X^1\Sigma^+\ |v = 0, J = 0\rangle$ at a temperature of 247 nK by utilizing a different two-photon pathway. An intermediate state of the spin-orbit coupled complex $B^1\Pi\ |v = 4\rangle \sim c^3\Sigma^+\ |v = 25\rangle$ is used and has the larger Franck-Condon factors for up- and down-leg coupling of STIRAP, as shown in Figure 1. The experiment starts from a mixture of ^{23}Na and ^{40}K atoms at 300 nK in an optical dipole trap. A magneto-association to a weak bounded Feshbach molecular state in the triplet state is applied by a fast ramping of the external magnetic field across a Feshbach resonance at 78.3 G. Then the sample of 3×10^4 molecules is transferred into the target deeply bound state in the singlet state by a STIRAP via an excited state, which has a character of a singlet state (92%) and triplet state (8%) mixing via spin-orbit coupling ξ_{Bc}=0.27 cm^{-1}. We obtain a spin-polarized molecular ensemble with yields of up to 2.2×10^4, and achieve a high one-way STIRAP transfer efficiency 75%. The sample of long-lived molecules is a good starting point for the quantum simulation, quantum information of ultracold molecules with long-range interaction.

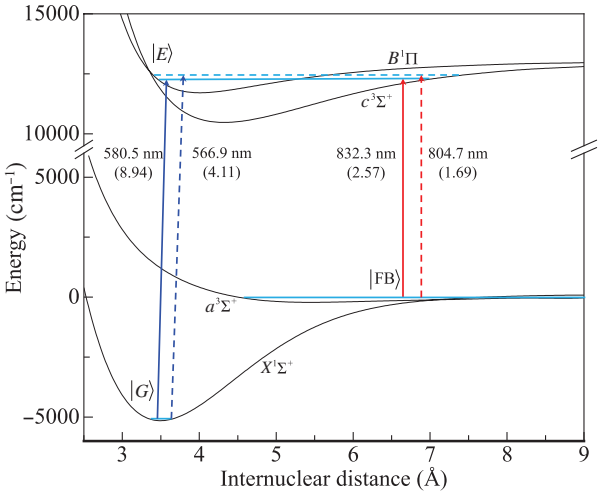

Figure 1 (Color online) Potential energy curves of ^{23}Na^{40}K molecules in the ground and excited states. The horizontal dashed line corresponds to the excited state in the mixed complex $B^1\Pi\ |v = 12\rangle \sim c^3\Sigma^+\ |v = 35\rangle$ used for the two-photon pathway with Raman lasers on 804.7 and 566.9 nm [19-21]. The horizontal solid line corresponds to the excited state in $B^1\Pi\ |v = 4\rangle \sim c^3\Sigma^+\ |v = 25\rangle$ used for the two-photon pathway with Raman lasers on 832.3 and 580.5 nm in this work. The Franck-Condon factors between the ground and excited states are presented in parentheses.

2 Produce of Feshbach molecules

Our experiment starts with a quantum degenerate mixture of Bose gas 1.5 × 10^5 ^{23}Na and Fermi gas 2.5 × 10^5 ^{40}K at 300 nK in an optical dipole trap at 1064 nm in the mixture state ^{23}Na$|1, 1\rangle$+^{40}K$|9/2, 9/2\rangle$ at 1 G [34-37].

To prepare the Feshbach molecules, we first transfer the ^{40}K atoms to the state $|9/2, -7/2\rangle$ at 26 G by Landau-Zener effect, then the magnetic field is ramped to 80.3 G in 10 ms. At this moment, the mixture is quickly prepared in the state ^{23}Na$|1, 1\rangle$+^{40}K$|9/2, -9/2\rangle$. A fast sweeping of the magnetic field is followed from 80.3 to 78 G at a rate of 1.15 G/ms during 2 ms, which is passed through the resonant point 78.3 G, and the Feshbach molecules $|FB\rangle$ of about 3 × 10^4 are prepared by the magneto-association method [27]. Then the magnetic field is quickly ramped to 72.4 G during 0.1 ms. To measure the Feshbach molecules, we dissociate the Feshbach molecules to the atoms by ramping the field from 72.4 to 80.3 G, and count the ^{40}K atoms in $|9/2, -9/2\rangle$ state after a time-of-flight (TOF) expansion. The time sequence has been shown in Figure 2.

Creating efficiency mainly depends on the spatial overlapping of dual-species atoms in density distributions [29, 38, 39]. Many methods have been developed, such as add an additional laser on 785 nm to increase the spatial overlap [29] or use a large Fermi gas to Bose gas number ratio [22, 26], which could significantly enhance the association efficiency.

Here, we found that the creating efficiency is also limited by the fast loss induced by ^{23}Na atoms in the creating process.

After the ramping, the Feshbach molecules and the remaining atoms of ^{23}Na and ^{40}K coexist in the sample. We need to remove the remaining atoms as soon as possible. A gradient field is quickly used to remove the atoms for preparing a pure sample of Feshbach molecules. To produce a gradient field B' along the direction of gravity at B_0=72.4 G, the currents in the pair of coils in the Helmholtz configuration are tuned by two silicon power transistors during 1 ms, where the sum of two currents $I_{\rm sum}$ remains fixed value, as shown in Figure 3.

$$\begin{aligned} B_0 &\propto I_{\rm sum} = I_{\rm down} + I_{\rm up}, \\ B' &\propto I_{\rm diff} = I_{\rm down} - I_{\rm up}, \end{aligned} \tag{1}$$

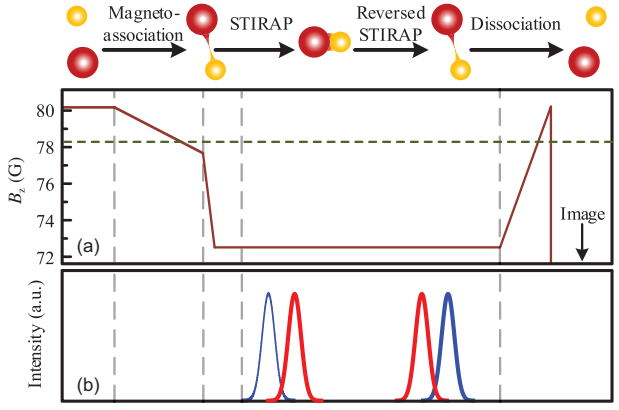

Figure 2 (Color online) An overview of the time sequence of the external magnetic field and the STIRAP lasers. (a) Magnetic field ramps for the association and dissociation of Feshbach molecules across the magnetic Feshbach resonance at 78.3 G (indicated by the horizontal dashed line), and subsequent imaging of ^{40}K after a few ms of time-of-flight (TOF) expansion. The brown-red curve represents magnetic field sweeps. (b) Laser intensity pulse sequence normalized to their individual intensity maximums in STIRAP and reversed STIRAP. Blue (red) Gaussian pulse for the Stokes (pump) beams.

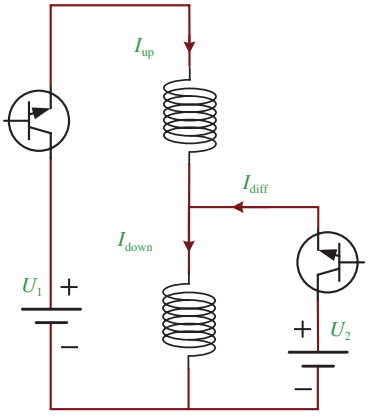

Figure 3 (Color online) Magnetic field control setup of a pair of coils operating at the Helmholtz configuration. The currents $I_{\rm up}$ and $I_{\rm down}$ in the up and down coils are turned by two silicon power transistors.

$I_{\rm up}$ and $I_{\rm down}$ are the currents in the up and down coils. This configuration of power supply for two coils can easily realizes to keep the bias magnetic field B_0=72.4 G constant, and at the same time ramp the gradient magnetic field B' quickly. Due to the atoms and molecules having different magnetic moments, the atoms are quickly separated from the molecules and escape from the trap. After a cleaning time of 20 ms, we could obtain pure Feshbach molecules at 251 nK. Due to the different trapping depths, the ^{23}Na atoms are firstly removed during 5 ms.

We first study the collision property of the mixture of Feshbach molecules and remaining atoms from molecules loss measurement by holding with different time and measuring the Feshbach molecules number. The loss rate of Feshbach molecules and ^{23}Na atoms is very large and limit the lifetime of the mixture to only 4.9 ms, as shown in Figure 4(a). After removing the remaining ^{23}Na atoms, the

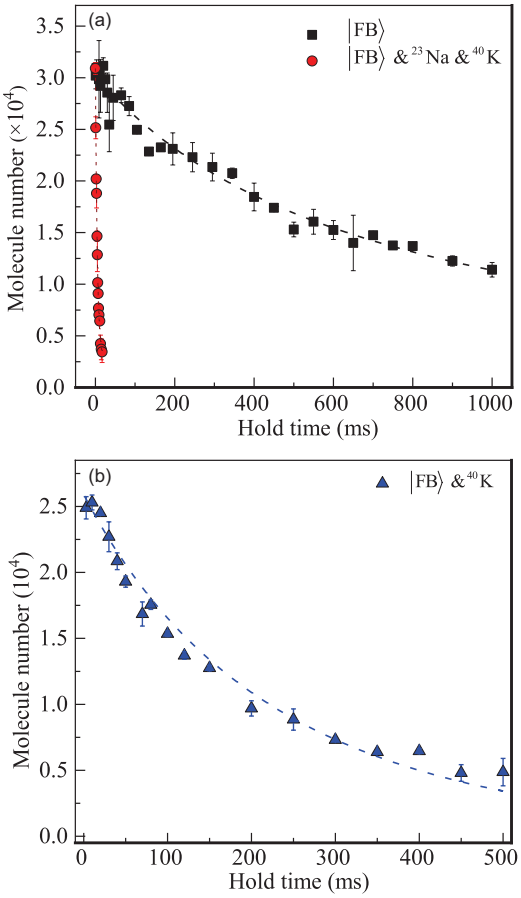

Figure 4 (Color online) Lifetime of ^{23}Na^{40}K Feshbach molecules. The measurement is performed at a magnetic field of 72.4 G. (a) The red circles (black squares) data points show the number of molecules as a function of hold time without (with) removing sodium atoms and potassium atoms. The red dashed line corresponds to exponential fits. The black dashed line corresponds to fits using the solution of eq. (2). (b) The blue triangles data points show the number of molecules as a function of hold time with potassium atoms. The blue dashed line corresponds to fits using the solution of eq. (2).

lifetime of molecules with ^{40}K is significantly increased to 156 ms, as shown in Figure 4(b). The lifetime of pure molecules is further up to 459 ms, which is significantly longer than that of the molecules by RF association [40]. Here the Feshbach molecules associated by the magneto-association method are nearly on the closed-channel fraction at 72.4 G, the molecules created by the Rf association are open-channel dominated. The fast loss in the case of the mixture ($|$FB$\rangle$+^{23}Na+^{40}K) could be attributed to the exothermic chemical reaction NaK + Na $\rightarrow$ Na_2 + K, in which the product dimers $^{23}Na_2$ with lower binding energy are produced [41].

The molecules decay could be modelled with the loss equation:

$$\dot{N}(t) = -\frac{k_2 \cdot N^2(t)}{V_{\rm eff}} - k_1 \cdot N(t), \tag{2}$$

where k_1 is one-body loss rate induced by the collisions with background gas or the remaining atoms ^{40}K, k_2 is two-body loss rate. The effective volume of the thermalized sample is given by $V_{\rm eff} = \left[4\pi k_{\rm B} T/\left(m\bar{\omega}^2\right)\right]^{3/2}$, and $\bar{\omega} = (\omega_x\omega_y\omega_z)^{1/3}$ is the mean trapping frequency and m is the mass for Feshbach molecules. We obtain the two-body loss rate coefficient of $1.07(2)\times10^{-12}$ cm^3/s at 251 nK by fitting the experimental data in case of pure molecules. The two-body loss rate is closed to the previous measured value [42], indicated that the Feshbach molecules at 72.2 G are deep in the non-halo regime. For the mixture of molecules and ^{40}K atoms, the one-body loss rate of 3.57(6) s^{-1} is obtained with the atomic mean density $\overline{n}_K \sim 4.56\times10^{12}$ cm^{-3}.

To reduce this loss mechanism in the process of producing Feshbach molecules by magneto-association, we optimize the sweeping rate of the magnetic field and decrease the optical depth at the same time. This step also gives a cooling effect, letting the hottest ^{23}Na atoms leave the trap under the effect of gravity and keeping the colder atoms stay at the trap to balance the loss and the production process. Now the long-lived Feshbach molecules about 3×10^4 at 251 nK in the spin-triplet state have been produced, being a good starting point for creating ultracold molecules at the rovibrational ground state.

3 STIRAP

For the STIRAP transfer Feshbach molecules to the rovibrational ground state, the spin-orbit coupled complex $B^1\Pi$ $|v=4\rangle \sim c^3\Sigma^+$ $|v=25\rangle$ is chosen as the excited intermediate state $|E\rangle$. A detailed study of this complex has been presented in ref. [43], they investigated the high resolution single-photon spectroscopy and pointed out that this complex has a spin-orbit coupling strength ξ_{Bc}=0.27 cm^{-1} and larger Franck-Condon factors for both pump and Stokes transitions.

In STIRAP, a high degree of phase coherence between a pair of Raman lasers is necessary. Here the pump laser operated at 832 nm couples the Feshbach molecule state $|$FB$\rangle$ and an intermediate excited state $|E\rangle$, and the Stokes laser at 580 nm couples the ground molecule state $|G\rangle$ and intermediate excited state, as shown in Figure 1. A schematic of the STIRAP laser system is shown in Figure 5. A pair of external cavity diode lasers (ECDL) being master lasers operated at 832 and 1160 nm is used for the pump and Stokes laser beams respectively. The output power of ECDL is divided into three different parts. A small part of the power (~100 μW) is split off for monitoring laser frequency using a wavelength meter. A part of the power (≈1 mW) is split off to be coupled into fiber electro-optical modulators (EOM) for locking of laser frequency to the ULE cavity mode.

To obtain the high degree of phase coherence between a pair of Raman lasers, we lock the two laser frequencies to an ultra-low expansion (ULE) cavity simultaneously using the Pound-Drever-Hall (PDH) technique [44]. The 100-mm-long ULE cavity is mounted in a vacuum chamber and coated for a finesse of 30800 at 1160 nm and 35200 at 832 nm, which also could be checked by the measurement of the lifetime of the lasers in the cavity. The back reflection lasers at 580 and 1160 nm from the cavity are detected by two resonant photodetectors (RPD) with a resonant frequency of 30 MHz, respectively. We apply two-tone modulations on the fiber EOMs, which greatly simplifies the STIRAP laser system. One of the two-tone modulations is used to continuously tune the frequencies of two STIRAP laser beams in half of the free spectral range (≈750 MHz) of the ULE cavity respectively, which creates a high-frequency sideband on the carrier light by applying a sideband modulation frequency f_2 ~300 MHz to fiber EOM for the light of 832 nm (f_4 ~715 MHz for the light of 1160 nm). Another tone modulation with PDH modulation frequency ($f_{1,3}$=30 MHz) is used for PDH locking, which creates a low-frequency sideband to the carrier light and the high-frequency sideband light. At the same time, this tone is mixed with the electric signal from RPD to generate an error signal for locking. The error signal is divided into two branches to the current of the diode lasers for the fast frequency correction, and to the piezo of the external cavity for slow frequency drift.

The main part of the power of ECDL operated at 832 nm is injected into a tapered amplifier (TA), which has an output power of 650 mW for the pump transition. The main part of the power of ECDL operated at 1160 nm is then injected into a Raman fiber amplifier (RFA) and frequency-doubled by second-harmonic generation (SHG) to generate the 580 nm laser of 300 mW for the Stokes transition. The

pump and Stokes laser beams are switched by two AOMs and coupled to polarization-maintaining fibers, sent to the experimental apparatus. Meanwhile, the AOMs can control laser pulse shape (Gaussian or square) for different purposes in the following experiment.

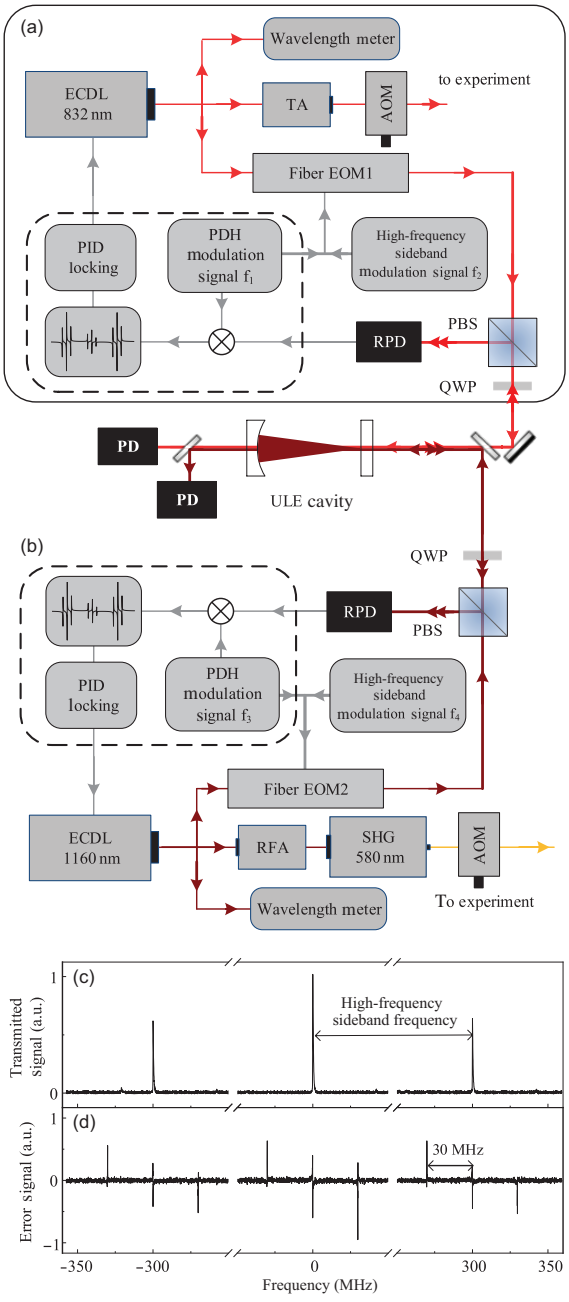

Figure 5 (Color online) STIRAP laser system for pump laser (a) and Stokes laser (b). A pair of ECDLs to provide laser at 1160 and 832 nm for the Stokes and pump transitions, respectively. The fiber EOMs are operated at multiple frequencies simultaneously for creating the sideband and modulating to generate the error signal, which is sent to a fast analogue servo module. The resonant photodetectors (RPD) pick up the reflection beams from ULE cavity. The photodetectors (PD) are used to monitor the transmission of the ULE cavity mode. The Stokes light at 1160 nm is injected into a Raman fiber amplifier and frequency-doubled by second-harmonic generation to generate the Stokes laser at 580 nm. The Stokes light and pump light are switched by AOMs and fiber-coupled respectively. (c) The transmitted signal through the ULE cavity shows the carrier light and two high-frequency sideband lights at 832 nm. (d) The corresponding PDH error signal.

To check the high degree of phase coherence between the two Raman lasers, we perform the two-photon dark state spectroscopy by measuring the remaining Feshbach molecules after illumination of a square shape of pump beam (72 μW) and Stokes beam (5 mW) with a flash time 0.05 ms. The high-resolution spectroscopy of the excited state of $^{23}Na^{40}K$ has been reported [43]. Here, the coupling beam ω_S is on resonance with an excited state in the coupling complex $B^1\Pi\ |v = 4, J = 1\rangle \sim c^3\Sigma^+\ |v = 25, J = 1\rangle$ with mixed singlet and triplet character ξ_{Bc}=0.27 cm^{-1}. The detuning of the pump beam ω_p is scanned by changing the high-frequency tone on fiber EOM to measure the number of remaining Feshbach molecules. Figure 6(a) shows the experimental data and the theoretical fit. The two-photon dark state spectroscopy could be described by the three-level model [24,45].

$$N = N_0 \exp\left(-t\Omega_p^2 \frac{4\gamma\delta^2}{\left|\Omega_S^2 + 2i\delta(\gamma + 2i\Delta)\right|^2}\right), \tag{3}$$

from the fitting, the coupling strength $\Omega_p = 2\pi \times 0.24$ MHz and Ω_S=$2\pi \times 10.6$ MHz are obtained, the linewidth γ=$2\pi \times 7.3$ MHz of intermediate state $|E\rangle$, which is the same order of the linewidth of the state reported in ref. [43]. A peak

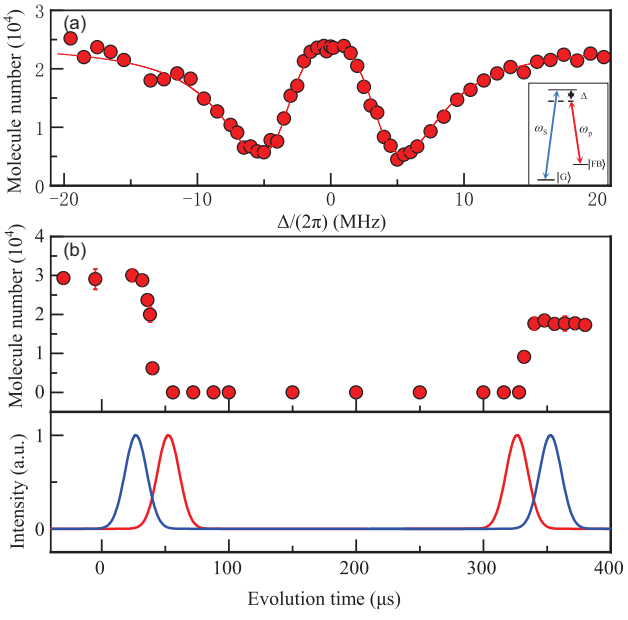

Figure 6 (Color online) (a) Two-photon dark state spectroscopy. The solid line shows the fitting based on eq. (3). We extract a peak pump Rabi frequency of Ω_p=$2\pi \times 0.24$ MHz and a peak Stokes Rabi frequency of Ω_S=$2\pi \times 10.63$ MHz from the fitting. The inset shows a three-level scheme of STIRAP. (b) Evolution of the number of Feshbach molecules during a round-trip STIRAP. The lower panel shows the time sequence of Stokes (blue) and pump (red) light pulses.

was observed with $\delta = \Delta$, which features there is a dark state in the system with a high degree of phase coherence between the two independent laser beams. The two-photon dark state spectroscopy means that we observe an absolute ground state $|G\rangle$.

Here, the two laser Raman beams are overlapped in space and propagate in the horizontal plane and perpendicular to the external magnetic field, which defines the quantization axis along the gravity direction. We could choose the laser polarization parallel or perpendicular to the quantization axis, which corresponds to the π or $(\sigma^+ + \sigma^-)$ transition. Different combinations of polarization of two STIRAP laser beams can prepare the ground state molecules in a specified hyperfine state. The initial Feshbach state has the total angular momentum projection m_F=−7/2. According to the optical transition selection rule, the ground state molecules in specific hyperfine levels with total spin projection $m_{F,G}$=$m_{I_{Na}} + m_{I_K}$=−11/2, −9/2, −7/2, −5/2 or −3/2 could be accessed by choosing different polarizations of STIRAP lasers and the distinct excited state with the quantum number $m_{F,E}$=−9/2, −7/2, or −5/2 [19, 20, 43].

4 Creation of ground state molecules

Now, we could use the STIRAP to transfer Feshbach molecules to the ground state. Here we chose the STIRAP process with the Stokes laser at 580.5 nm and pump laser at 832.3 nm and the intermediate state in the coupling complex $B^1\Pi\ |v = 4, J = 1\rangle \sim c^3\Sigma^+\ |v = 25, J = 1\rangle$ is used. The time sequence of the STIRAP laser beams pulse is shown in Figure 2(b), where a pair of Gaussian pulse shapes for the pump and Stokes laser is used

$$P(t) = P_0 e^{-\left(\frac{t-t_0}{\zeta}\right)^2}, \tag{4}$$

where the peak power P_0 and the pulse delay t_0 could be independently controlled by the AOMs. The pulse duration time $\tau = 2\sqrt{ln2}\cdot\zeta$ is defined as the full width at half maximum of the Gaussian pulse.

Figure 6(b) shows the STIRAP transfer the Feshbach molecules to the ground state. The figure includes the STIRAP light pulse sequence (lower panel) and the populations of the Feshbach molecules during the STRAIP sequence (upper panel). Starting with Feshbach molecules, the molecules are transferred to the ground state after the STIRAP pulse. At that moment, the molucules are populated in the ground state and no Feshbach molecules are probed. To image the ground state molecules, the number of molecules is determined by using a reversed-STIRAP to transfer back to Feshbach molecules and immediately dissociating the Feshbach molecules into the mixture state ^{23}Na$|1, 1\rangle$+^{40}K$|9/2, -9/2\rangle$. And then the ^{40}K atoms are detected by the TOF image. All parameters of molecules are obtained from the information of ^{40}K atoms. In this process, we suppose the ^{40}K atoms perfectly transmit the information of the sample of ground state molecules. Here, we could measure ^{40}K atoms of about 1.7×10^4 at 247 nK, and determine the one-way STIRAP efficiency η ~75%. It is supposed that the reversed-STIRAP and STIRAP have the same conversation efficiency. We estimate that about 2.2×10^4 at 247 nK ground state molecules are created.

We prepare the molecules in the hyperfine state $|m_{I,Na}, m_{I,K}\rangle = |1/2, -4\rangle$ in the absolute ground state (see the inset in Figure 7(a)) and study the one-way STIRAP

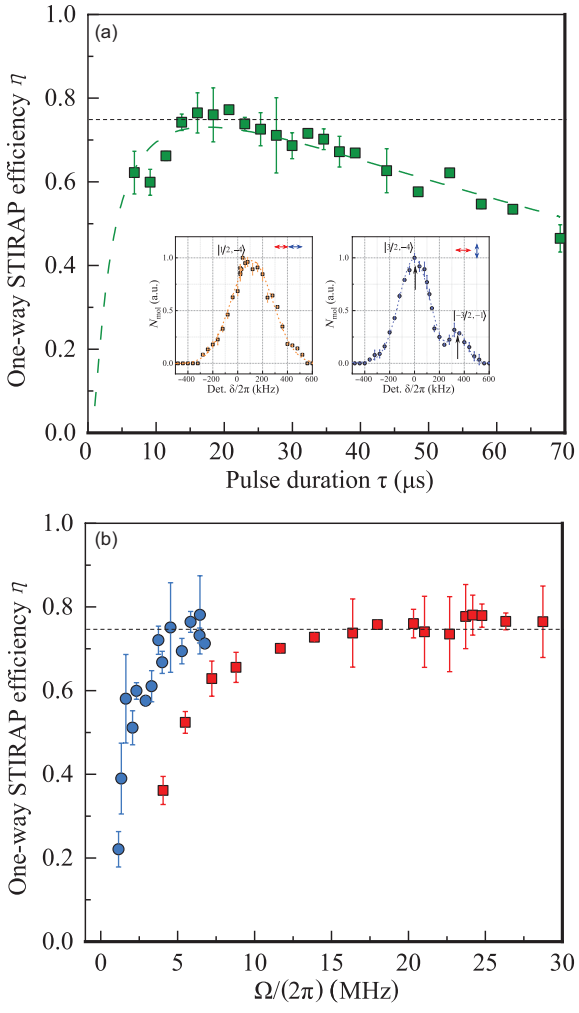

Figure 7 (Color online) One-way STIRAP efficiency depends on the pulse duration time (a) and Rabi frequencies (b). (a) We denote the FWHM of the Gaussian shape of the beam intensity as the pulse duration. The dashed line is the fit of eq. (5) to the experimental data with Ω_p=2π × 26.9 MHz and Ω_S=2π × 6 MHz. The insets show the STIRAP spectrums obtained by scanning the Stokes laser with different polarizations with the pump laser on resonance. (b) Red squares (blue circles) indicate the data recorded with the peak Rabi frequency of pump (Stokes) beam vs. one-way STIRAP efficiency. Error bars denote the standard deviation of the mean of three experimental runs.

efficiency η on the function of the Gaussian pulse width τ, shown in Figure 7(a). One can see that the efficiency can achieve the maximum value of about 75% at the width of 18 μs and decrease as the duration time is longer. This relationship could be fitted by the theory developed in refs. [46, 47] to consider the effects of the laser noise.

$$\eta(\tau) = \exp\left(-\frac{\pi^2\gamma}{\Omega^2\tau} - \frac{\tau}{4}\left(D_p + D_S + \Gamma_p + \Gamma_S\right)\right), \quad (5)$$

where τ is the pulse duration and γ is the linewidth of the intermediate excited state, D_p, D_S are the linewidth of STIRAP lasers at 832 and 580 nm, $\Gamma_{p,S}$ corresponds to the background noise of the two laser beams. To increase the STIRAP efficiency, a filter cavity in the STIRAP laser system has been used to decrease the laser noise and significantly improve the one-way STIRAP efficiency [20].

Figure 7(b) shows the function of laser coupling strength on the one-way STIRAP efficiency. It is found that the efficiency reaches the saturation point when the coupling strength $\Omega_p > 2\pi \times 15$ MHz and $\Omega_S > 2\pi \times 5$ MHz.

5 Conclusion

In conclusion, we have created an ultracold sample of about 2.2×10^4 fermionic molecules ^{23}Na^{40}K in the absolute ground state $X^1\Sigma^+ |v = 0, J = 0\rangle$. The time sequence of the external magnetic field and the STIRAP laser setup have been described in detail. The collision property of Feshbach molecules and atoms was also studied, and a long-lived sample of Feshbach molecules was observed. We have demonstrated a new two-photon pathway from the Feshbach molecular state to the rovibrational ground state via the coupled complex $B^1\Pi |v = 4\rangle \sim c^3\Sigma^+ |v = 25\rangle$, which has the larger Franck-Condon factors for STIRAP. We also found that the high one-way STIRAP transfer efficiency can reach 75%, and believed that it could be greatly increased by reducing the laser noise. In combination with the external electrical field, magnetic field, and optical lattices, the molecules in their absolute rovibrational ground state serve as an ideal starting point for the study of many-body physics and quantum simulation with long-range interaction.

This work was supported by the Science and Technology Innovation 2030-Major Project (Grant No. 2021ZD0302003), the National Key Research and Development Program of China (Grant Nos. 2022YFA1404101, 2021YFA1401700, and 2018YFA0307601), the National Natural Science Foundation of China (Grant Nos. 12034011, 92065108, 11974224, 12022406, and 12004229), and the Fund for Shanxi 1331 Project Key Subjects Construction, and Tencent (Xplorer Prize).

Conflict of interest The authors declare that they have no conflict of interest.

1 L. D. Carr, D. DeMille, R. V. Krems, and J. Ye, New J. Phys. **11**, 055049 (2009), arXiv: 0904.3175.
2 G. Quéméner, and P. S. Julienne, Chem. Rev. **112**, 4949 (2012).
3 M. A. Baranov, M. Dalmonte, G. Pupillo, and P. Zoller, Chem. Rev. **112**, 5012 (2012).
4 N. R. Cooper, and G. V. Shlyapnikov, Phys. Rev. Lett. **103**, 155302 (2009), arXiv: 0907.3080.
5 G. M. Bruun, and E. Taylor, Phys. Rev. Lett. **101**, 245301 (2008), arXiv: 0809.1422.
6 S. F. Yelin, K. Kirby, and R. Côté, Phys. Rev. A **74**, 050301 (2006), arXiv: quant-ph/0602030.
7 M. He, C. Lv, and Q. Zhou, Adv. Quantum Tech. **5**, 2100117 (2022).
8 J. L. Bohn, A. M. Rey, and J. Ye, Science **357**, 1002 (2017), arXiv: 1708.02806.
9 D. Demille, Phys. Rev. Lett. **88**, 067901 (2002), arXiv: quant-ph/0109083.
10 D. Mitra, K. H. Leung, and T. Zelevinsky, Phys. Rev. A **105**, 040101 (2022), arXiv: 2204.12373.
11 A. Micheli, G. K. Brennen, and P. Zoller, Nat. Phys. **2**, 341 (2006), arXiv: quant-ph/0512222.
12 N. R. Hutzler, H. I. Lu, and J. M. Doyle, Chem. Rev. **112**, 4803 (2012).
13 D. J. Nesbitt, Chem. Rev. **112**, 5062 (2012).
14 F. Schreck, and K. Druten, Nat. Phys. **17**, 1296 (2021), arXiv: 2209.01026.
15 C. Chin, R. Grimm, P. Julienne, and E. Tiesinga, Rev. Mod. Phys. **82**, 1225 (2010).
16 T. Takekoshi, L. Reichsöllner, A. Schindewolf, J. M. Hutson, C. R. Le Sueur, O. Dulieu, F. Ferlaino, R. Grimm, and H. C. Nägerl, Phys. Rev. Lett. **113**, 205301 (2014), arXiv: 1405.6037.
17 P. K. Molony, P. D. Gregory, Z. Ji, B. Lu, M. P. Köppinger, C. R. Le Sueur, C. L. Blackley, J. M. Hutson, and S. L. Cornish, Phys. Rev. Lett. **113**, 255301 (2014), arXiv: 1409.1485.
18 M. Guo, B. Zhu, B. Lu, X. Ye, F. Wang, R. Vexiau, N. Bouloufa-Maafa, G. Quéméner, O. Dulieu, and D. Wang, Phys. Rev. Lett. **116**, 205303 (2016), arXiv: 1602.03947.
19 J. W. Park, S. A. Will, and M. W. Zwierlein, Phys. Rev. Lett. **114**, 205302 (2015), arXiv: 1505.00473.
20 R. Bause, A. Kamijo, X. Y. Chen, M. Duda, A. Schindewolf, I. Bloch, and X. Y. Luo, Phys. Rev. A **104**, 043321 (2021), arXiv: 2106.10089.
21 H. Yang, D. C. Zhang, L. Liu, Y. X. Liu, J. Nan, B. Zhao, and J. W. Pan, Science **363**, 261 (2019), arXiv: 1807.11160.
22 L. De Marco, G. Valtolina, K. Matsuda, W. G. Tobias, J. P. Covey, and J. Ye, Science **363**, 853 (2019).
23 A. Schindewolf, R. Bause, X. Y. Chen, M. Duda, T. Karman, I. Bloch, and X. Y. Luo, Nature **607**, 677 (2022), arXiv: 2201.05143.
24 F. Seeßelberg, N. Buchheim, Z. K. Lu, T. Schneider, X. Y. Luo, E. Tiemann, I. Bloch, and C. Gohle, Phys. Rev. A **97**, 013405 (2018), arXiv: 1709.00902.
25 A. Yang, S. Botsi, S. Kumar, S. B. Pal, M. M. Lam, I. Čepaitė, A. Laugharn, and K. Dieckmann, Phys. Rev. Lett. **124**, 133203 (2020), arXiv: 1908.02703.
26 J. Cao, H. Yang, Z. Su, X. Y. Wang, J. Rui, B. Zhao, and J. W. Pan, Phys. Rev. A **107**, 013307 (2023), arXiv: 2208.09620.
27 K. K. Ni, S. Ospelkaus, M. H. G. de Miranda, A. Pe'er, B. Neyenhuis, J. J. Zirbel, S. Kotochigova, P. S. Julienne, D. S. Jin, and J. Ye, Science **322**, 231 (2008), arXiv: 0808.2963.
28 F. Wang, X. He, X. Li, B. Zhu, J. Chen, and D. Wang, New J. Phys. **17**, 035003 (2015), arXiv: 1502.03869.
29 M. Duda, X. Y. Chen, A. Schindewolf, R. Bause, J. von Milczewski, R. Schmidt, I. Bloch, and X. Y. Luo, Nat. Phys. **19**, 720 (2023), arXiv: 2111.04301.
30 P. S. Żuchowski, and J. M. Hutson, Phys. Rev. A **81**, 060703 (2010), arXiv: 1003.1418.
31 M. Aymar, and O. Dulieu, J. Chem. Phys. **122**, 204302 (2005), arXiv: quant-ph/0502059.
32 A. Gerdes, O. Dulieu, H. Knöckel, and E. Tiemann, Eur. Phys. J. D

65, 105 (2011).
33 A. Christianen, M. W. Zwierlein, G. C. Groenenboom, and T. Karman, Phys. Rev. Lett. **123**, 123402 (2019), arXiv: 1905.06846.
34 Z. Li, Z. Gu, Z. Shi, P. Wang, and J. Zhang, Chin. Phys. B **32**, 023701 (2023).
35 Z. Shi, Z. Li, P. Wang, K. Sadiq Nawaz, L. Chen, Z. Meng, L. Huang, and J. Zhang, J. Opt. Soc. Am. B **38**, 1229 (2021).
36 Z. Shi, Z. Li, P. Wang, Z. Meng, L. Huang, and J. Zhang, Chin. Phys. Lett. **35**, 123701 (2018), arXiv: 1803.05108.
37 X. Wang, Z. Shi, Z. Li, Z. Gu, P. Wang, and J. Zhang, J. Quantum Opt. **28**, 8 (2022).
38 J. Herbig, T. Kraemer, M. Mark, T. Weber, C. Chin, H. C. Nägerl, and R. Grimm, Science **301**, 1510 (2003).
39 T. D. Cumby, R. A. Shewmon, M. G. Hu, J. D. Perreault, and D. S. Jin, Phys. Rev. A **87**, 012703 (2013), arXiv: 1212.0903.
40 C. H. Wu, J. W. Park, P. Ahmadi, S. Will, and M. W. Zwierlein, Phys. Rev. Lett. **109**, 085301 (2012), arXiv: 1206.5023.
41 K. M. Jones, S. Maleki, S. Bize, P. D. Lett, C. J. Williams, H. Richling, H. Knöckel, E. Tiemann, H. Wang, P. L. Gould, and W. C. Stwalley, Phys. Rev. A **54**, R1006 (1996).
42 M. Duda, X.-Y. Chen, R. Bause, A. Schindewolf, I. Bloch, and X.-Y. Luo, arXiv: 2202.06940.
43 J. W. Park, S. A. Will, and M. W. Zwierlein, New J. Phys. **17**, 075016 (2015), arXiv: 1505.01835.
44 R. W. P. Drever, J. L. Hall, F. V. Kowalski, J. Hough, G. M. Ford, A. J. Munley, and H. Ward, Appl. Phys. B **31**, 97 (1983).
45 M. Fleischhauer, A. Imamoglu, and J. P. Marangos, Rev. Mod. Phys. **77**, 633 (2005).
46 L. P. Yatsenko, V. I. Romanenko, B. W. Shore, and K. Bergmann, Phys. Rev. A **65**, 043409 (2002).
47 L. P. Yatsenko, B. W. Shore, and K. Bergmann, Phys. Rev. A **89**, 013831 (2014).